2017

Tire-Pavement Interaction Modeling: Hyperelastic Tire and Elastic Pavement

Jaime Hernandez
Marquette University, jaime.hernandez@marquette.edu

Imad L. Al-Qadi
University of Illinois - Urbana-Champaign

Road Materials and Pavement Design, Vol. 18, No. 5 (2017). DOI.

Tire–pavement interaction modelling: hyperelastic tire and elastic pavement

Jaime A. Hernandez
Illinois Center for Transportation, University of Illinois at Urbana-Champaign, 1611 Titan Drive, Rantoul, IL 61866, USA
Imad L. Al-Qadi
Illinois Center for Transportation, University of Illinois at Urbana-Champaign, 1611 Titan Drive, Rantoul, IL 61866, USA

Abstract

The interaction between deformable tire and pavement was studied using the validated finite element model; the full understanding of tire–pavement contact has implications for pavement damage prediction and pavement life-cycle assessment (fuel consumption estimation). The tire's rubber and reinforcement were considered hyperelastic and linear elastic, respectively, with material constants obtained from the tire manufacturer (rubber) and laboratory testing (reinforcement). On the other hand, the pavement was assumed linear elastic supported by linear elastic springs. This assumption was made as a first step to examine the impact of using a deformable-on-deformable tire–pavement

system to predict energy in the tire and contact stresses. The effect of the pavement stiffness on contact area, tire deflection, three-dimensional contact stresses, surface deflection, internal energy of the tire and its components, the work performed by the contact forces, and dissipation caused by friction was also studied. The elastic modulus of the pavement affected the contact area, while the elastic constants of the springs were more relevant for tire deflection. In addition, stiffness of the pavement had a varying effect on each component of the three-dimensional contact stresses: vertical contact stresses remained almost constant and longitudinal ones were the most affected. The symmetry of the surface deflection decreased and the friction dissipation increased 10.2% as the elastic modulus changed from the smallest to the highest value. Finally, the work performed by the vertical contact forces was significantly higher than by the in-plane loads, and the stiffness of the pavement affected rolling resistance force, which is related to fuel consumption.

Keywords:

contact stresses, tire modelling, rolling resistance, fuel consumption, finite elements, Hyperelastic, deformable bodies

Introduction

According to the American Society of Civil Engineers (ASCE), 32% of America's major roads are in poor or mediocre condition (2013). In addition, the White House seeks to achieve 20% reduction in fuel consumption in semi-trucks fabricated after 2018 as part of its Climate Action Plan (2014). These two seemly very different statements have one common element: tire–pavement interaction.

It is assumed based on conventional road analysis that contact stresses acting in the vertical direction have constant magnitude. However, the study of tire–pavement interaction shows stresses transferred to the road in the three directions. Even more, various researches have demonstrated the relevant impact of three-dimensional (3-D) contact stresses on pavement responses and, consequently, on pavement design. For instance, Novak, Birgisson, and Roque (2003a, 2003b) considered the 3-D contact stresses measured in a pavement model and found the near-surface stress-states different from the conventional assumption; that is, the contact stresses were larger in magnitude, more localised, and with lower confinement near the tire's edge. Al-Qadi and Yoo (2007) developed a validated 3-D finite element pavement model, incorporating the measured 3-D contact stresses and moving load. The surface tangential contact stresses increased potential for the development of top-down cracking, primary rutting, and fatigue damage.

On the other hand, tire numerical models have been applied to study rolling resistance, temperature distribution, tire-road interaction, noise generation, and tire performance for over four decades (Ghoreishy, 2008). Rolling resistance is particularly important. When a vehicle is moving, the energy provided by fuel is spent overcoming five actions: rolling resistance, drag forces, internal friction in the vehicle, gravitational forces, and inertial forces (Michelin of Americas, 2003). This becomes even more relevant when taking into consideration that transportation is responsible for using 70% of the oil in the United States (The White House, 2014). Currently, work is underway to predict fuel consumption of a vehicle by analysing pavement responses without explicit consideration of tires or vehicles (Shakiba, Ozer, Ziyadi, & Al-Qadi, 2016).

Not many studies have combined tire and pavement in a single model. For instance, Al-Qadi and Wang used the decoupled approach, where a tire model was used to predict 3-D contact stresses, which later on were used as input for a 3-D pavement model to predict pavement responses and calculate pavement damage (Al-Qadi & Wang, 2011). Wang and Roque coupled tire and pavement in a single model and computed pavement responses (Wang & Roque, 2011). However, the analysis was static and material properties of both tire and pavement were assumed linear elastic. In addition, Xia developed a tire-terrain finite element model to study soil compaction and tire mobility. The tire component of the model did not include material properties measured in the laboratory or accurate geometry, and it was not validated using experimental measurements (Xia, 2011). Recently, Srirangam et al. developed a thermomechanical tire–pavement model focused on predicting temperature distribution in various regions of the tire (Srirangam, Anupam, Scarpas, & Kasbergen, 2014). Wollny et al. used a two-stage approach to model tire–pavement interaction, where the contact forces resulting from the tire contacting a rigid surface are used as input of a pavement model (Wollny, Behnke, Villaret, & Kaliske, 2016). At the same time, the resulting pavement deformation was used to update the surface contacted by the tire. The procedure was repeated until the difference in contact forces between of two consecutive iterations is small.

This paper combines both tire and pavement in a single finite element model. The validated tire model considered hyperelastic rubber and linear elastic reinforcement with material constants provided by the tire manufacturer and obtained from laboratory testing, respectively. In addition, accurate tire geometry was used. The pavement model was simplified; it consisted of a linear elastic deformable body supported by elastic springs on its bottom and side faces. The tire–pavement model was generated in three phases: axisymmetric tire, three-dimensional monotonic, and rolling. The tire inflation pressure was applied in the axisymmetric phase of the analysis, while the load was applied at the tire's axis during the generation of the three-dimensional model. A torque of magnitude zero and a constant speed of 8 km/h were applied at the tire's axis to perform the free rolling analysis. The main contribution of this study lies in the analysis of tire and pavement as deformable bodies in a couple fashion. First, the effect of pavement flexibility on the 3-D contact stresses and contact area, which has relevant consequence in the analysis of flexible pavements, is studied. Second, phenomena such as surface deflection, work performed by contact forces, and dissipation caused by friction forces are detailed, which are related to rolling resistance force and fuel consumption. Even though the viscoelastic nature of asphalt concrete is relevant when studying rolling resistance and fuel consumption, this research focused on the effect of surface deflection on the variables related to the deflection-based method to calculate a pavement's contribution to rolling resistance.

Finite element model

Tire and pavement composed the finite element model. Physical measurements defined the cross-section and distribution of materials in the tire (rubber and reinforcement). Hyperelastic behaviour was considered for rubber using the Mooney–Rivlin model, with material constants provided by the tire manufacturer. Additionally, reinforcement was assumed linear elastic. The modulus of elasticity of the reinforcement was the slope of the stress–strain curve after subjecting the specimens to tensile load (ASTM D882). The pavement was a deformable 100 × 600 × 3600 mm linear elastic block with modulus of elasticity E; linear elastic springs were assigned on each side of the pavement.

Even though subgrade inertia and damping greatly influence responses of roads subjected to moving load, pavement stresses and strains are not the main focus of this research. Consequently, and in order to obtain a computationally manageable model, the pavement was simplified as a deformable elastic body supported on elastic springs. The simplified pavement was a deformable 100 × 600 × 3600 mm linear elastic block with modulus of elasticity E; linear elastic springs were assigned on each side of the pavement. The length of 3600 mm was selected so that at least one full rotation of the tire was obtained. The 100-mm thickness and 600-mm width provided the least amount of finite elements that resulted in comparable surface deflection as the full pavement model.

The magnitude of spring's constants was different on each face of the pavement and was determined based on a full tire–pavement model (Figure 1). The pavement was composed by three layers: asphalt concrete (AC), granular base, and subgrade. Each layer's thickness changes depending on the type of pavement considered. In the case of a thick pavement, the thickness of the AC and base layers were 300 and 350 mm, respectively. For a thin pavement, the same thicknesses were 100 and 200 mm. Regarding material properties, the AC layer was assumed linear elastic with modulus varying between 102 and 105 MPa. Assuming AC as linear elastic material instead of viscoelastic is not expected to have a negative consequence on the conclusions of this study because the main focus is not pavement behaviour. Subgrade characterisation was given by the Drucker–Prager model, while the base was considered nonlinear anisotropic for a thin pavement and linear elastic for a thick pavement. For a thin pavement, the stress level in the base layer is significant, so the stress-dependency of the resilient modulus becomes relevant. That is not the case for thick pavements, where the stress levels in the base are low and the difference between linear and nonlinear models is not significant.

Figure 1. Full tire–pavement model.

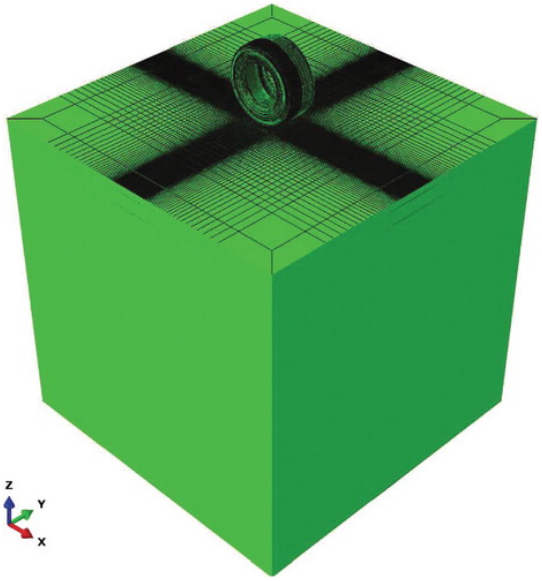

The full tire pavement model was subjected to a monotonic tire loading of magnitude 44.4 kN and tire inflation pressure of 758 kPa (Figure 1). The magnitude of the spring constants was calculated as the average of the stresses in the perpendicular direction divided by the average displacement in the same direction. For instance, the spring in the *z*-direction was obtained by dividing the average ratio between the stress in the *z*-direction 100 mm under the pavement surface by the *z*-displacement at

the same depth. The magnitude of the spring constant for thin and thick pavements and various elastic moduli of the AC layer are presented in Table 1.

Table 1. *k*-Values for thin and thick pavements.

	K (MPa/mm)					
	Thick pavement			Thin pavement		
Modulus (MPa)	x	y	z	x	y	z
E1 = 10^5	585.68	649.13	2.22	355.54	413.66	0.43
E2 = 10^4	58.44	69.95	0.87	20.02	29.12	0.20
E3 = 10^3	7.60	8.58	0.44	2.14	3.22	0.15
E4 = 10^2	0.79	1.15	0.21	0.33	1.58	0.14

The analysis consists of three phases: axisymmetric tire, 3-D monotonic, and rolling analysis. Material properties, cross-section geometry, boundary conditions, and tire inflation pressure were defined in the axisymmetric phase (Figure 2). The axisymmetric model was revolved with respect to the tires axis to generate the 3-D tire. After creating the 3-D tire and the pavement, they were brought to contact and the load was applied. Finally, free-rolling analysis was performed using ABAQUS by applying a constant speed of 8 km/h and a torque of zero magnitude at the tire's axis (Figure 3). To improve computational efficiency, friction was only defined in the final phase (free-rolling analysis) using the Coulomb model with coefficient of friction of 0.3. It is noteworthy to mention that: (i) tire–pavement friction is influenced by several factors such as pavement texture, temperature, viscoelastic properties of tire and pavement, contact pressure, speed, and slip ratio, among others; and (ii) the material models considered, linear elastic and hyperelastic, are not sensitive to speed. In addition, the influence of speed on the friction coefficient was also omitted. Consequently, tire speed is not expected to have any effect on the conclusions inferred from the proposed model.

Figure 2. Axisymmetric model.

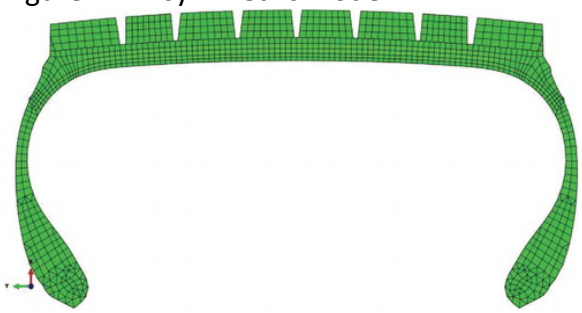

Figure 3. Simplified tire–pavement finite element model: (a) rigid surface and (b) deformable surface.

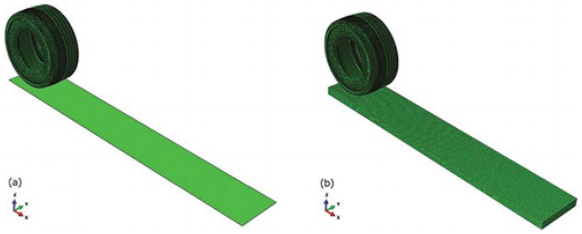

Cartesian elements were used along the circumference of the tire. In addition, hybrid and rebar elements modelled rubber incompressibility and tire reinforcement, respectively. Mesh sensitivity analysis determined the optimum size and distribution of finite elements based on the computational time and accuracy. The optimum mesh was the one with strain energy within ±5% of the one of a very fine mesh and the least amount of elements. Finally, the pavement was meshed with full-integration cubic elements with a 20 mm side.

The tire's finite element model was validated using measured contact area and deflection. A good agreement between contact area and deflection was observed (mean average percentage error of 4.2% and 8.5%, respectively). More details regarding the tire model are presented by Hernandez and Al-Qadi (2016).

The applied load and tire inflation pressure were fixed at 44.4 kN and 758 kPa. The elastic modulus of the pavement varied between 102 and 105 MPa, while the elastic foundation constant was determined based on static analysis of the full tire–pavement model as previously described. Analysis was also performed for the tire contacting the analytical rigid surface, referred to herein as the rigid case.

Contact area and deflection

Figure 4 shows the variation of contact area (Ac.) and tire deflection (δ) for various values of E. Each plot has four lines representing: (i) tire rolling on a rigid pavement; (ii) monotonic tire loading on a thin pavement; (iii) monotonic tire loading on a thick pavement; and (iv) rolling tire on a simplified thick pavement.

Figure 4. Variation of contact area and deflection with type of pavement (thin or thick) and modulus of deformable surface.

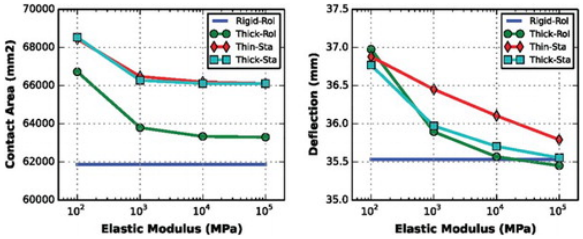

For static and rolling analysis, most of the influence of E occurred between E = 10^2 and 10^3 MPa: For thick and thin pavements in the static analysis, Ac reduced 3.3% and 2.9%, respectively, if E increased from 10^2 to 10^3 MPa. The diminution in contact area became less than 0.5% for the other values of E. When the elastic modulus of the deformable block exceeded 10^4 MPa, Ac was almost constant. In other words, there is a value starting from which the contact area becomes independent of the

pavement stiffness. When the tire deforms, it tries to match the deformed shape of the pavement. Consequently, the created curvature increases the amount of contact points between the pavement and the tire, resulting in an increment in contact area. For the rigid case, no such deformation of the pavement exists; so Ac was the least possible for the given applied load and tire inflation pressure.

The contact area for thin and thick pavements and static analysis are almost coincidental for all values of elastic modulus E, indicating higher influence of the pavement's surface's stiffness on Ac rather than the rest of the pavement structure. In addition, for rolling analysis, the contact area approached a constant value as a pavement's stiffness increased, but the value did not match the rigid case. Even the stiffest pavement experienced surface deflection, slightly affecting Ac.

The variation of tire deflection δ (average deflection in the case of rolling analysis) with respect to the elastic modulus of the pavement is shown in Figure 4. For a thin pavement, the static deflection changed almost linearly with E in the logarithmic scale, and decreased from 36.9 mm when E = 10^2 to 35.8 mm when E = 10^5, a reduction of 3.0%. The difference in deflection between static and rolling analyses for a thick pavement was not significant and followed the same trend. Consequently, in contrast to contact area, deflection would not greatly depend on rolling condition but on pavement type.

Three-dimensional contact stresses

The relevance of a pavement's stiffness on each component of the 3-D contact stresses was determined taking the stiffest case (E = 10^5 MPa) as baseline. Comparisons were made on two aspects: First, the variation of contact stresses along the length at a representative location across the tire; and second, the contact stresses at each point on the contact patch.

The variation of the 3-D contact stresses (vertical, longitudinal, and transverse) along the length of tire contact for the various E -values is shown in Figure 5. Figure 5(a) focuses on the vertical pressure distribution, which results from the superposition of the tire inflation pressure and vertical pressure values that depend on the structural characteristic of the tire and operating conditions (Clark, 1971). The analysis was performed considering the same tire inflation pressure and applied load on the same tire; so the only changing factor was the operating conditions (pavement in this study).

Figure 5. Effect of pavement stiffness on 3-D contact stresses: (a) vertical contact stresses; (b) transverse contact stresses; and (c) longitudinal contact stresses ($E1 > E2 > E3 > E4$).

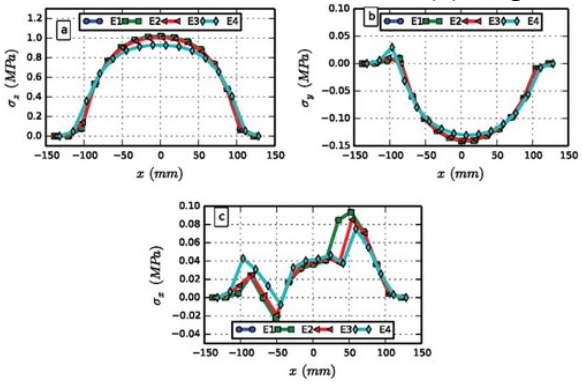

Figure 5(c) emphasises the longitudinal contact stresses σx. The stresses in this direction for free rolling are defined by the relative displacement in the travelling direction between the contact points

(Clark, 1971). For tire rolling on the stiffest surface, the relative displacement is maximum because there is no deformation on the pavement. If the tire is rolling on a deformable surface, deformation occurs on the pavement, the relative displacement between the tire and the surface decreases, and σx diminishes. Consequently, the longitudinal contact stresses for the deformable surface are mainly defined by its stiffness. Transverse contact stresses, which are shown in Figure 5(b), are mainly caused by the restriction on tread displacement in the direction perpendicular to traffic (Clark, 1971). When tire inflation pressure is low and applied load is high, the forces transferred through the tires sidewall might influence σy. As for σx, the rigid surface imposed the highest constraint on movement, and, consequently, provided the highest transverse contact stresses. The boundary conditions imposed on the pavement did constrain displacements in the transverse direction; so the magnitude of σy did not change significantly when flexibility of pavement was modified.

The contact stresses in each direction for the foot region were stored in arrays. The root-mean-square error and the coefficient of determination (RSME and R^2, respectively) were used to compare the various arrays, taking the stiffest case as reference. Figure 6 compares the vertical contact stresses with the stiffest case for all the values of E (as defined in Table 1) and the thick pavement. If the elastic modulus of the pavement was high, *RMSE* would not change; however, if E was low, the RSME would increase 4.6 times from 0.005 to 0.023 MPa when changing the elastic modulus from 10^2 to 10^3 MPa. Finally, the maximum RSME was 0.023 MPa, 2.3% the maximum vertical contact stresses in Figure 6.

Figure 6. Comparison of vertical contact stresses with respect to the stiffest case.

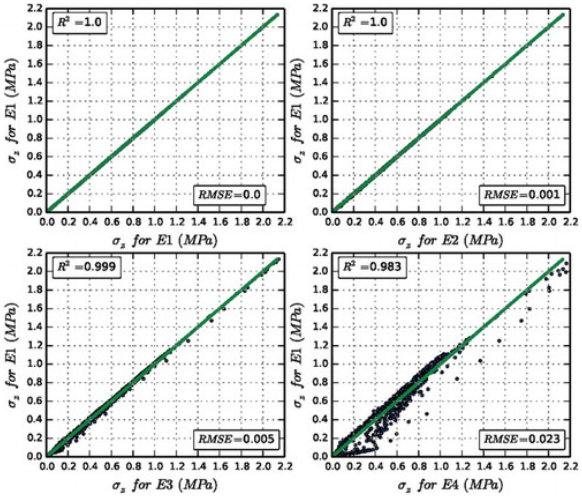

Figure 7 presents the same comparison as in Figure 6, but for the case of longitudinal contact stresses, the component most affected by E. The agreement with the reference case decreased as the stiffness of the pavement decreased; $R^2$and RSME became 0.845 and 0.003 MPa (31.6% the maximum value in Figure 5(c)), respectively. As previously mentioned, the longitudinal contact stresses during free rolling are mainly determined by the relative displacement at the contact points between the tire and the pavement in the travelling direction, which increases as the stiffness of the pavement decreased.

Figure 7. Comparison of longitudinal contact stresses with respect to the stiffest case.

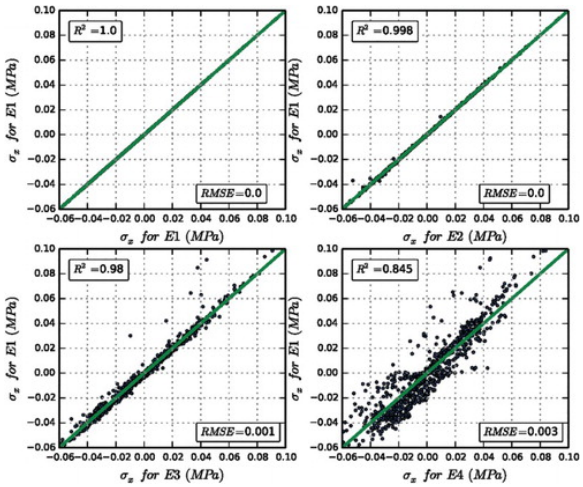

Finally, the effect of the pavement's stiffness on the transverse contact stresses is presented in Figure 8. Once more, the highest difference was found for the most compliant pavement with R^2 = .973 and RSME = 0.004, 35% the maximum magnitude in Figure 8. Even though the percentage of the maximum is higher than for σx, the coefficient of determination is not as low.

Figure 8. Comparison of transverse contact stresses with respect to the stiffest case.

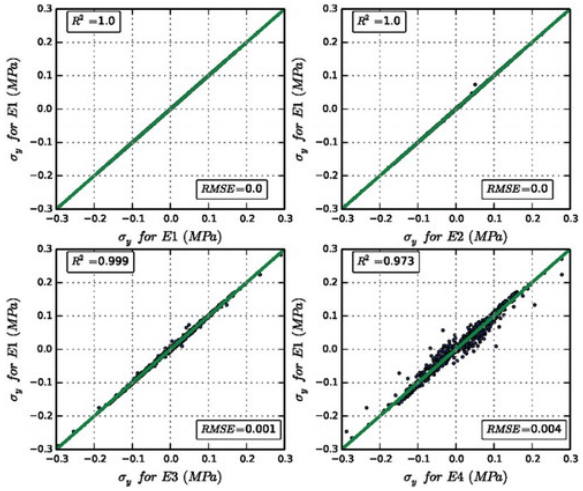

In summary, stiffness of a pavement is more relevant for longitudinal contact stresses, followed by transverse and then vertical contact stresses. This is mainly due to the relevance of relative displacement between contact points at the tire–pavement interface on the in-plane contact stresses.

Tire's internal energy

The study of energy balance and the components of the tire–pavement system is relevant for fuel consumption and environmental impact of truck tires. Figure 9 shows the variation of the internal energy in the tire (ALLIEtire) and its components as a function of the elastic modulus. The total height of the bars represents the energy in the whole tire, and it is divided into the contribution of each component. The internal energy slightly decreased from 0.2358 kJ when E = 10^5 to 0.2328 kJ when E = 10^2 MPa, a diminution of 1.3%. The contribution of the tire elements to ALLIEtire for each pavement stiffness did not significantly change either; however, the internal energy of the components did

change with respect to the stiffest case. For instance, ALLIEtread remained at about 15.0% of ALLIEtire for the range of E-values, but it decreased 5.3% from 0.0357 kJ when E = 10^5 to 0.0338 kJ when E = 10^2 MPa. Consequently, as the internal energy in the tire components changes, the energy dissipated by the tire due to modifications in the pavement might change as well. This finding contradicts the assumption of non-dissipative tire when calculating structure-induced rolling resistance (Chupin, Piau, & Chabot, 2013).

Figure 9. Internal energy in the tire by component.

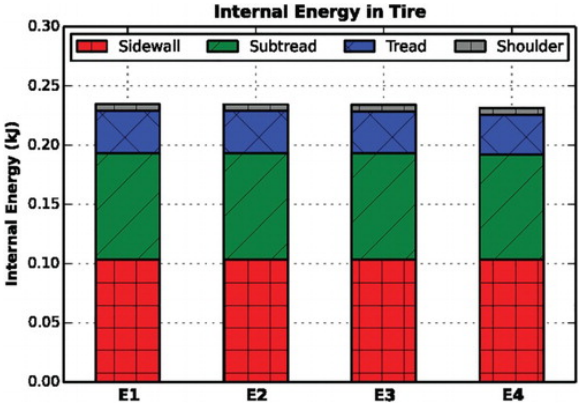

Surface deflection

A sample of the deflection along the pavement's surface is shown in Figure 10. To check the symmetry of the deformed shape with respect to the point of maximum deflection, the areas under the curve before ($A1$) and after ($A2$) the peak deflection were compared. If the curve is symmetric, $A1 = A2$. For each E-value, the deflection along the wheel-path was calculated for thirty-one paths across the pavement's surface and the average $A1$ was computed. The ratio $A1/A$ changed as the stiffness of the pavement decreased. For the stiffest pavement, the average ratio was 0.504, which indicates a symmetric deformed shaped. However, as E approached 10^2, the average ratio became 0.512, with a maximum of 0.526.

Figure 10. Deflection sample along the moving direction.

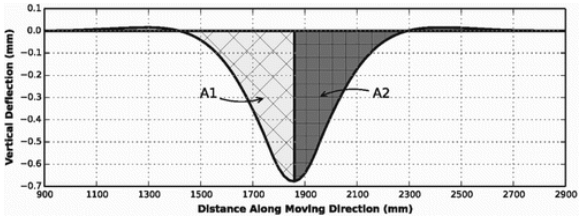

The distribution of contact pressure mainly depends on four parameters: (i) support provided by the sidewall to the tread, (ii) bending and shear deformation of the thread, (iii) tread buckling, and (iv) tread's normal compliance/stiffness (Clark, 1971). In addition, the distribution of vertical contact stresses is only symmetric under static loading. If the tire is rolling, the contact pressure shifts in the moving direction; so the peak values are not at the centre of the contact length. The magnitude of the shift increased as the speed increased, and the shear deformation is crucial in explaining such behaviour.

Since contact pressure is not symmetric, unsymmetrical behaviour of the surface deflection is also expected, as it was found. It should be noted that the analyses were performed at slow-moving load, so higher asymmetry can be obtained at higher speeds. Consequently, a point in the pavement surface may have different loading and unloading paths as the tire travels over it.

Table 2 shows the variation of the rolling resistance force (Rx), the vertical reaction (Rz), the rolling resistance coefficient (Crr), and the eccentricity (e) with respect to the elastic modulus of the pavement. The eccentricity was defined as the distance from the centre of the tire to the location of the vertical contact stresses' resultant. A reduction of 5.2% and 13.1% in Fx and e is observed when decreasing E from 10^5 to 10^2 MPa. This indicates that, even though tire and pavement are elastic and do not dissipate energy, the rolling resistance force and consequently the fuel consumption are changed by the characteristics of the pavement. The trend and values in Table 2 most likely will change once variables such as viscoelasticity of the pavement and tire are considered, and phenomena like the tire always being on an uphill slope are addressed (Louhghalam, Akbarian, & Ulm, 2013, 2014). This work is currently underway by the authors.

Table 2. Variation of coefficients of rolling resistance with elastic modulus.

E (MPa)	R_x (N)	R_y (N)	R_z (N)	C_{rr} (°/°°)	e (mm)
1.0 x 10^5	-20.31	558.35	44398.7	-0.4574	0.2301
1.0 x 10^4	-20.30	557.65	44698.9	-0.4573	0.2312
1.0 x 10^3	-20.15	557.37	44399.4	-0.4539	0.2185
1.0 x 10^2	-19.24	547.30	44411.3	-0.4333	0.1999

Work performed by contact forces and frictional dissipation

When performing the life cycle assessment of a road infrastructure, the pavement structure contributes to rolling resistance. The contribution can be calculated using two equivalent methods, one based on the viscoelastic dissipation of the pavement structure and the other based on pavement surface deflection (Chupin et al., 2013; Louhghalam et al., 2013; Pouget, Sauzéat, Benedetto, & Olard, 2012). The deflection-based method involves the calculation of the work performed by contact forces, so understanding contact forces and surface displacements as the tire travels on the pavement surface is relevant.

Figures 11–13 present the variation of nodal force and displacement with respect to time along the vertical, longitudinal, and transverse directions, respectively. The plots correspond to one node in the pavement surface and the most compliant pavement. The continuous line represents the portion of time the tire is approaching the node until it reached the maximum load magnitude, while the dashed line indicates the unloading phase. The figures also give the force–displacement relationship for the node; the area enclosed by the force–displacement curve is related to the work performed by the contact loads.

Figure 11. Variation of vertical force and displacement with time for *E*4: (a) vertical force vs. time; (b) vertical displacement vs. time; and (c) vertical force vs. vertical displacement (continuous lines represent loading and dashed ones unloading).

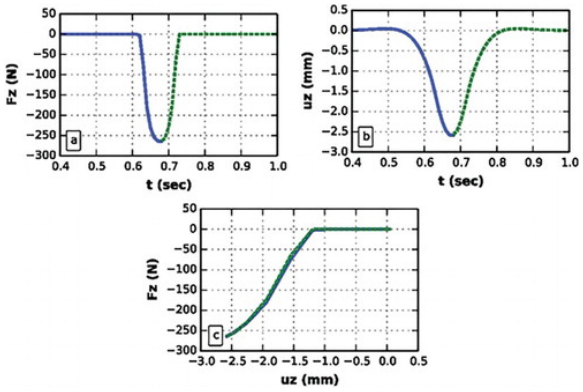

Figure 12. Variation of longitudinal force and displacement with time for E4: (a) longitudinal force vs. time; (b) longitudinal displacement vs. time; and (c) longitudinal force vs. longitudinal displacement (continuous lines represent loading and dashed ones unloading).

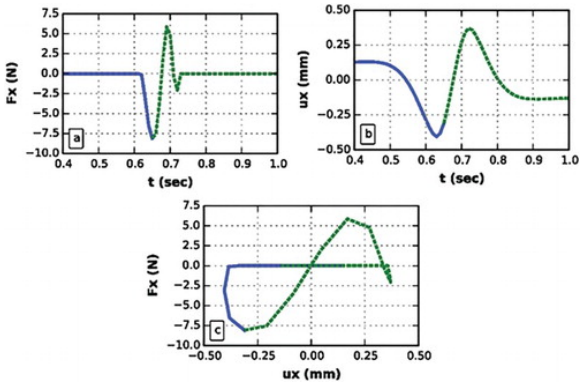

Figure 13. Variation of transverse force and displacement with time: (a) transverse force vs. time; (b) transverse displacement vs. time; and (c) transverse force vs. transverse displacement (continuous lines represent loading and dashed ones unloading).

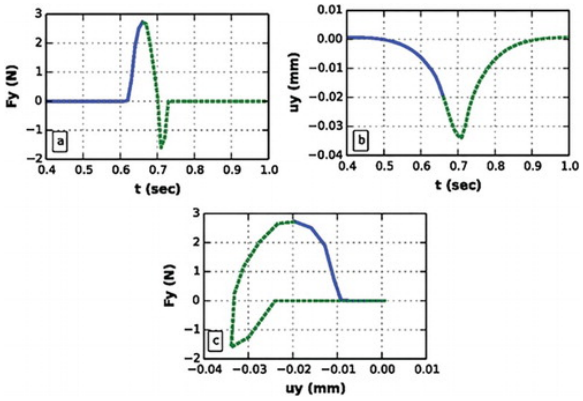

As observed in Figure 11, the maximum value of vertical displacement (uz) and vertical reaction force (Fz) occurred at the same time. The loading and unloading paths are very close to each other, and numerical calculation of the area between the two curves provides a negligible value. Because of the slight asymmetry of the vertical contact forces, the loading and unloading paths were different, causing a small enclosed area. However, higher asymmetry can be seen when considering a viscoelastic

pavement subjected to high temperatures and slow moving loads. It is also noted that, due to the bending stiffness of the pavement, the lack of vertical force does not imply zero vertical deflection. This observation is particularly important for the in-plane directions.

The behaviour along the in-plane directions was different than the previous case. Figure 12 presents the same information as Figure 11 but in the longitudinal direction x. The sign of the reaction force Fx and the displacement ux changed as the tire passed the node, and the time at maximum longitudinal reaction force did not coincide with the time at maximum longitudinal displacement (the time discrepancy was higher in the transverse direction as seen in Figure 13). Slip at the contact between the tire and the pavement, which for free rolling is localised at the beginning and end of the contact patch, may cause the mismatch between maximum force and displacement. In addition, for the considered node, the loading and unloading paths in the *x* and *y* directions were dissimilar. Along the longitudinal direction, the load-deflection curve showed negative and positive enclosed areas which were equal in magnitude for the stiffest pavement but somewhat different for the most compliant case. The area enclosed was not very symmetric in the *y* direction.

The work performed by the external forces for a segment of the pavement fully subjected to loading and unloading ($1000\ mm\ \leq x \leq\ 2000$ or $0.39\ s\ \leq t \leq\ 0.95\ s$) was calculated. For each node, the force–deflection curve was obtained and the enclosed area calculated. Afterwards, the enclosed areas for all the nodes were added and the results are shown in Figure 14. The work performed by the vertical contact forces (Wz) was orders of magnitude higher than in the longitudinal and transverse directions (W_x and y, respectively). In addition, in the vertical direction, W_z increased to a plateau until the tire was fully on the section of pavement examined. As the tire left the examined section, the energy decreases back to almost zero. The behaviour was different along the in-plane direction, where a constant value remained after the tire passed the considered surface segment. The work performed by the vertical contact forces was mostly positive; however, for the x and y directions, negative W_x and W_z were observed. Negative work indicates the contact reaction force and the displacement are in opposite directions.

Figure 14. Work performed by contact forces in three principal directions: (a) work performed by Fx; (b) work performed by Fy; and (c) work performed by Fz (continuous lines represent loading and dashed ones unloading).

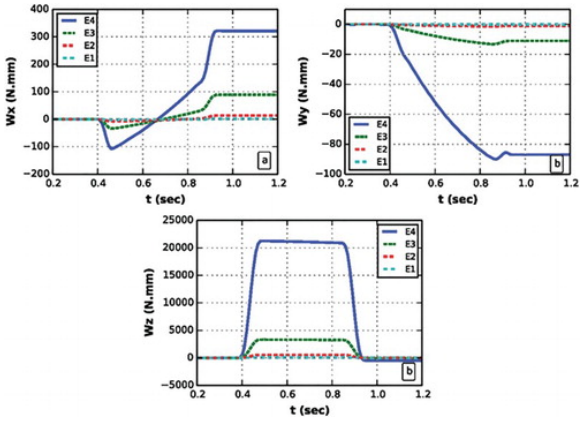

The energy dissipated by the friction forces started from zero at the beginning of the analysis and accumulated as the tire moved over the pavement. Since material properties for tire and pavement

were elastic, friction force is the only source of dissipation. Friction is closely related to the slip occurring between the tire and the pavement, which accounts for less than 5% of the rolling resistance (Michelin of Americas, 2003). Figure 15 presents the change of the frictional dissipation (ALLFD) at the end of the analysis for the various values of elastic modulus. ALLFD increased as E increased due to higher relative motion between tire and pavement. The difference in energy dissipated by friction between E = 10^2 and E = 10^5 was 9.3%.

Figure 15. Frictional dissipation at the end of the analysis.

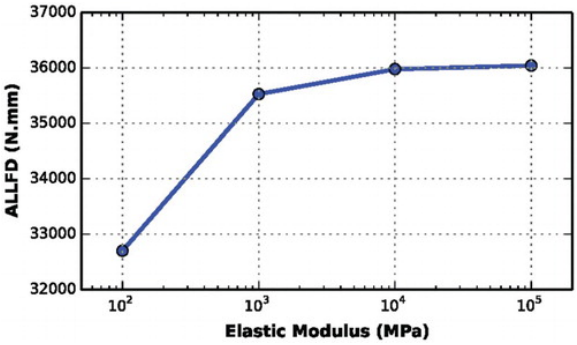

Conclusions

The interaction between the deformable tire and pavement was studied using the finite element method. Four cases of surface stiffness and tire at free rolling composed the parametric study. Variation of contact area, tire deflection, 3-D contact stresses, surface deflection, internal energy in the tire, work performed by contact forces, and frictional dissipation with pavement stiffness were analysed. The contact area mainly changed between the two smallest elastic moduli, with the highest change being around 3% for thin and thick pavements. Tire deflection depended on the pavement type, and its variation was also around 3%.

The vertical contact stresses were not affected by the stiffness of the pavement; however, the longitudinal component was the most affected by the pavement's stiffness. Because of the ability of the pavement to deform, relative displacement of the points at the contact patch decreased, thus reducing the longitudinal contact stresses at free rolling. The discrepancy between rigid and deformable cases was quantified using the root-mean-square error and the coefficient of determination. This difference was mainly seen for the in-plane contact stresses, with the lowest R^2 and highest RMSE observed in the longitudinal direction.

Regarding the internal energy in the tire, the pavement elastic modulus did not change the share of each tire component on the total internal energy of the tire, but it did affect the value of each component up to 5.3%. In addition, it was proved that the surface deflection is not fully symmetric, and the degree of asymmetry changed with the elastic modulus of the pavement. The work performed by the vertical contact forces was significantly higher than the in-plane components, and it was recovered after removing the tire loading. The work of the in-plane contact forces was negative in some instances because the load and the displacement pointed in opposite directions. The stiffness of the pavement increased the dissipation caused by frictional forces by 9.3%. Finally, the rolling resistance force decreased 5.2% from the stiffest to the most compliant pavement even though the tire and the pavement were elastic. This trend will most likely change after including variables such as

viscoelasticity of the tire and the pavement. In addition, the values reported in this study may be magnified once variables such as the pavement's and tire's viscoelasticity, speed, and temperature are included.

Even though the obtained differences are less than 10% and seem irrelevant, they correspond to a single load application. The difference might accumulate and propagate for actual traffic and result in a significant difference in analysis such as fatigue cracking.

Disclosure statement

No potential conflict of interest was reported by the authors.

Additional information

Funding

The authors would like to acknowledge the financial support of the Federal Highway Administration. This study used the Extreme Science and Engineering Discovery Environment (XSEDE), which is supported by National Science Foundation [grant number ACI-1053575].

References

1. Al-Qadi, I. L., & Wang, H. (2011). Prediction of tire pavement contact stresses and analysis of asphalt pavement responses: A decoupled approach. *Journal of the Association of Asphalt Paving Technologists*, *76*, 289–316.
2. Al-Qadi, I. L., & Yoo, P. J. (2007). Effect of surface tangential contact stresses on flexible pavement response. *Journal of the Association of Asphalt Paving Technologists*, *76*, 663–692.
3. American Society of Civil Engineers. (2013). *2013 report card for America's infrastructure*. http://www.infrastructurereportcard.org. [Google Scholar]
4. Chupin, O., Piau, J.-M., & Chabot, A. (2013). Evaluation of the structure-induced rolling resistance (DRR) for pavements including viscoelastic material layers. *Materials and Structures*, *46*(4), 683–696. doi: 10.1617/s11527-012-9925-z
5. Clark, K. (Ed.). (1971). *Mechanics of pneumatic tires*. Washington, DC: Department of Commerce.
6. Ghoreishy, M. H. R. (2008). A state of the art review of the finite element modelling of rolling tyres. *Iranian Polymer Journal*, *17*(8), 571–597.
7. Hernandez, J. A., & Al-Qadi, I. L. (2016). Hyperelastic modeling of wide-base tire and prediction of its contact stresses. *Journal of Engineering Mechanics*, *142*(2), 04015084-1–04015084-11.
8. Louhghalam, A., Akbarian, M., & Ulm, F. J. (2013). Flügge's conjecture: Dissipation-versus deflection-induced pavement–vehicle interactions. *Journal of Engineering Mechanics*, *140*(8), 04014053-1–04014053-10.
9. Louhghalam, A., Akbarian, M., & Ulm, F.-J. (2014). Scaling relationships of dissipation-induced pavement-vehicle interactions. *Transportation Research Record: Journal of the Transportation Research Board*, *2457*, 95–104. doi: 10.3141/2457-10
10. Michelin of Americas. (2003). *The tyre rolling resistance and fuel savings* (Report no.). Michelin of Americas.

11. Novak, M., Birgisson, B., & Roque, R. (2003a). Near-surface stress states in flexible pavements using measured radial tire contact stresses and ADINA. *Computer and Structures*, *81*, 859–870. doi: 10.1016/S0045-7949(02)00413-3

12. Novak, M., Birgisson, B., & Roque, R. (2003b). Tire contact stresses and their effects on instability rutting of asphalt mixture pavements three-dimensional finite element analysis. *Transportation Research Record: Journal of the Transportation Research Board*, *1853*, 150–156. doi: 10.3141/1853-17

13. Pouget, S., Sauzéat, C., Benedetto, H. D., & Olard, F. (2012). Viscous energy dissipation in asphalt pavement structures and implication for vehicle fuel consumption. *Journal of Materials in Civil Engineering*, *24*(5), 568–576. doi: 10.1061/(ASCE)MT.1943-5533.0000414

14. Shakiba, M., Ozer, H., Ziyadi, M., & Al-Qadi, I. L. (2016). Mechanics based model for predicting structure-induced rolling resistance (SRR) of the tire-pavement system. *Mechanics of Time-Dependent Materials*, 1–22. doi:10.1007/s11043-016-9313-0

15. Srirangam, S., Anupam, K., Scarpas, A., & Kasbergen, C. (2014). Development of a thermomechanical tyre-pavement interaction model. *International Journal of Pavement Engineering*, *16*(8), 1–9.

16. The White House. (2014). *Improving the fuel efficiency of American trucks* (Report No.) The White House.

17. Wang, G., & Roque, R. (2011). Impact of wide-based tires on the near-surface pavement stress states based on three-dimensional tire-pavement interaction model. *Road Materials and Pavement Design*, *12*(3), 639–662. doi: 10.1080/14680629.2011.9695264

18. Wollny, I., Behnke, R., Villaret, K., & Kaliske, M. (2016). Numerical modelling of tyre–pavement interaction phenomena: Coupled structural investigations. *Road Materials and Pavement Design*, *17*(3), 563–578. doi: 10.1080/14680629.2015.1094399

19. Xia, K. (2011). Finite element modeling of tire/terrain interaction: Application to predicting soil compaction and tire mobility. *Journal of Terramechanics*, *48*(2), 113–123. doi: 10.1016/j.jterra.2010.05.001